Kinetic Evidence for the PsaE-Dependent Transient Ternary Complex Photosystem I/Ferredoxin/Ferredoxin:NADP$^+$ Reductase in a Cyanobacterium†

Jasper J. van Thor,‡,§ Torsten H. Geerlings,‡ Hans C. P. Matthijs,§ and Klaas J. Hellingwerf*,‡

Laboratory for Microbiology, E.C. Slater Institute, and Laboratory for Microbiology, ARISE/MB, University of Amsterdam, Nieuwe Achtergracht 127, 1018 WS Amsterdam, The Netherlands

Received February 12, 1999; Revised Manuscript Received June 17, 1999

ABSTRACT: A mutant of *Synechocystis* PCC 6803, deficient in *psaE*, assembles photosystem I reaction centers without the PsaE subunit. Under conditions of acceptor-side rate-limited photoreduction assays in vitro (with 15 μM plastocyanin included), using 100 nM ferredoxin:NADP$^+$ reductase (FNR) and either *Synechocystis* flavodoxin or spinach ferredoxin, lower rates of NADP$^+$ photoreduction were measured when PsaE-deficient membranes were used, as compared to the wild type. This effect of the *psaE* mutation proved to be due to a decrease of the apparent affinity of the photoreduction assay system for the reductase. In the *psaE* mutant, the relative *petH* (encoding FNR) expression level was found to be significantly increased, providing a possible explanation for the lack of a phenotype (i.e., a decrease in growth rate) that was expected from the lower rate of linear electron transport in the mutant. A kinetic model was constructed in order to simulate the electron transfer from reduced plastocyanin to NADP$^+$, and test for possible causes for the observed change in affinity for FNR. The numerical simulations predict that the altered reduction kinetics of ferredoxin, determined for the *psaE* mutant [Barth, P., et al., (1998) *Biochemistry 37,* 16233−16241], do not significantly influence the rate of linear electron transport to NADP$^+$. Rather, a change in the dissociation constant of ferredoxin for FNR does affect the saturation profile for FNR. We therefore propose that the PsaE-dependent transient ternary complex PSI/ferredoxin/FNR is formed during linear electron transport. Using the yeast two-hybrid system, however, no direct interaction could be demonstrated in vivo between FNR and PsaE fusion proteins.

The primary photochemical reaction in photosystem I (PSI)[1] is the transmembrane transport of an electron from a chlorophyll *a* dimer to stromal acceptors, after which the chlorophyll dimer cation is rereduced by either plastocyanin or cytochrome *c*. The cyanobacterial photosystem I consists of at least 14 subunits and resembles the core of the more complex chloroplast PSI reaction center (*1*, *2*). The heterodimeric core is formed by PsaA and PsaB, and is believed to bind approximately 100 chlorophyll *a* molecules, that form the reaction center's light harvesting antenna. Excitation energy is transferred via red-shifted chlorophyll *a* species to the primary donor P700. Its excited state then leads to a charge separation, leaving a positive charge on P700, and transferring an electron to the primary acceptor A_0, which is thought to be a chlorophyll *a* monomer with an approximate midpoint potential for reduction of −1050 mV (*3*). The electron is subsequently transferred to a transient intermediate, A_1, that has been identified as a phylloquinone [vitamin K_1, E_m: −800 mV; (*4*, *5*)]. The next intermediate acceptor is the [4Fe-4S] cluster F_X (E_m: −750 mV). PsaC is a stroma-exposed, 9 kDa ferredoxin-like subunit of PSI that carries two [4Fe-4S] clusters, F_A and F_B [E_m: −540 and −590 mV, respectively; (*6*)], functioning as electron carriers between F_X and ferredoxin.

The crystal structure of *Synechococcus* photosystem I was solved at 6 Å (and recently at 4 Å) resolution (*1*, *7*, *8*). Although it is not known which cluster is F_A or F_B, two [4Fe-4S] clusters were assigned with respective distances of 15 and 22 Å to F_X. In the 6 Å structure, the stroma-exposed subunits PsaC, PsaD, and PsaE were not unambiguously assigned. Rather, electron microscopy of mutant photosystem I particles has led to the localization of these subunits in trimeric PSI particles of *Synechocystis* PCC 6803 (*9*). PsaC is positioned centrally on the PsaAB heterodimer. PsaE is positioned toward the edge of the particle, in close proximity to PsaC. PsaD is positioned opposite of PsaC, oriented more toward the center of the trimeric particle. This topological model was confirmed by protease accessibility studies, using the same set of mutants (*10*). The combination of these data allowed discrimination between PsaA and PsaB in the structure, which was not possible from the 4 Å crystal structure. It was found that PsaE mainly covers the PsaA

† This study was supported by the Life Sciences Foundation (SLW), which is subsidized by The Netherlands Organization for Scientific Research (NWO).

* Corresponding author. Fax: +31-20-5257056. E-mail: K.Hellingwerf@chem.uva.nl.

‡ E.C. Slater Institute.

§ ARISE/MB.

[1] Abbreviations: Tris, tris(hydroxymethyl)aminomethane; Hepes, 4-(2-hydroxyethyl)-1-piperazineethanesulfonic acid; Tricine, *N*-[tris-(hydroxymethyl)methyl]glycine; DCMU, 3-(3,4-dichlorophenyl)-1,1-dimethylurea; IPTG, isopropyl β-D-galactoside; PMSF, phenylmethanesulfonyl fluoride; DCPIP, 2,6-dichlorophenolindophenol; DAD, diaminodurene; TMPD, tetramethyl-*p*-phenylenediamine; 3-AT, 3-amino-1,2,4-triazole; X-Gal, 5-bromo-4-chloro-3-indolyl-β-D-galactopyranoside; PC, plastocyanin; FNR, ferredoxin−NADP$^+$ reductase; FNR(ox), oxidized species of FNR; FNR(sq), one-electron-reduced (semiquinone) species of FNR; FNR(red), reduced species of FNR; PSI, photosystem I.

10.1021/bi9903502 CCC: $18.00
Published on Web 09/09/1999

subunit, whereas PsaD covers PsaB. Moreover, chemical cross-linking studies confirm this arrangement; PsaC has been shown to cross-link to both PsaD and PsaE (*11*).

Ferredoxin has been shown to cross-link to the PsaD subunit of photosystem I (*12*). Analysis of electron micrographs of a covalently cross-linked complex of ferredoxin and *Synechocystis* PCC 6803 trimeric photosystem I particles revealed its binding site (*13*). Ferredoxin was found to cross-link to a site in direct contact with the ridge that is made up by PsaE, -C, and -D, distal to the 3-fold axis of the PSI trimer, covering PsaB. A similar experiment was performed with a cross-linked complex between *Synechococcus* 7002 PSI trimers and flavodoxin, showing that ferredoxin and flavodoxin bind approximately the same site (*14*). The solution structure of the recombinant PsaE subunit was determined by NMR, and found to consist mainly of β-strands (*15*). Recently, the Psa subunits C, D, and E were also identified in the 4 Å crystal structure of *Synechococcus elongatus* PSI (*1*). In combination, the results of the crystallographic, electron microscopic, chemical cross-linking, and NMR studies now provide a clear picture of the organization of the stromal subunits of PSI.

The *psaE* gene has been deleted both in *Synechocystis* PCC 6803 (*16*, *17*) and in *Synechococcus* PCC 7002 (*18*). Surprisingly, no effect of this mutation on the growth rate of these mutants was observed under conditions of photoautotrophic growth (*16*, *18*). Photoheterotrophic growth, however, is abolished in the *Synechococcus* mutant (*18*) and is slightly slower in the *Synechocystis* mutant (*19*). This impairment has been attributed to a deficiency in the photosystem I dependent route of cyclic electron transfer (*18*). The unperturbed photoautotrophic growth of the mutant, nevertheless, suggests that linear electron transport mediated by photosystem I is largely unaffected by the mutation. However, in vitro assays suggest that ferredoxin reduction by PsaE-less photosystem I may be deficient to some extent (*17*, *20*, *21*). Recently, it was determined that the most notable effect of the *psaE* mutation on photosystem I of *Synechocystis* PCC 6803 is a 100-fold increase of the dissociation constant for (*Synechocystis* PCC 6803) ferredoxin, which is mainly due to an increased off-rate of the complex (*22*).

The PsaE subunit has been found to cross-link to ferredoxin:$NADP^+$ reductase in photosystem I reaction centers of barley, isolated according to a specific protocol that yields highly active preparations containing approximately 0.4 molar equiv of FNR relative to P700 (*23*). Falzone et al. (*15*) note that in higher plants the positively charged N-terminal region of PsaE is exposed, whereas both its N- and its C-terminal regions were shown to be buried in *Synechocystis* PCC 6803 PSI (*17*). Falzone et al. (*15*) propose that the N-terminal region interacts with acidic residues of FNR, and explain the apparent absence of interaction in the cyanobacterial system (no FNR is copurified with PSI) in these terms.

Here we report on the detailed analysis of PSI-mediated linear electron transfer from reduced plastocyanin to $NADP^+$, in thylakoid membranes of wild type and a *psaE* mutant of *Synechocystis* PCC 6803. The experimental data obtained suggest the existence of a transient ternary complex composed of PSI, ferredoxin, and FNR, that is affected by the presence of the PsaE subunit of photosystem I. The stability of this complex may be smaller than in the case of barley PSI. However, a direct interaction between FNR and PsaE could not be demonstrated with the yeast two-hybrid system.

MATERIALS AND METHODS

Strains and Growth Conditions. Wild-type *Synechocystis* PCC 6803 and the *psaE* mutant (*17*) were cultured at 34 °C in BG11 medium (*24*) with continuous illumination of white fluorescent light (Philips TL 32), at an intensity of 70 $\mu E \cdot m^{-2} \cdot s^{-1}$. Kanamycin (50 μg/mL) was supplemented for culturing of the *psaE* mutant. Agitation was provided by continuous bubbling with air. Cultures grown for the isolation of membranes were harvested at high optical density, corresponding to a chlorophyll *a* concentration of about 10 μg/mL (approximately 10^8 cells/mL).

Analytical Procedures. Chlorophyll *a* concentration was determined after extraction with methanol at room temperature of either a cell pellet or a concentrated suspension of thylakoid membranes. The extinction coefficient at 665 nm divided by 76 yields the chlorophyll *a* concentration in milligrams per milliliter (*25*). The molar extinction coefficients used for ferredoxin:$NADP^+$ reductase were 10 700 cm^{-1} [at 458 nm; (*26*)], for flavodoxin 9500 cm^{-1} [at 466 nm; (*27*)], and for plastocyanin 4500 cm^{-1} [at 597 nm; (*28*)].

Cloning Procedures. The *Synechocystis* PCC 6803 *petH* gene (*29*) was amplified by PCR with Pwo polymerase (Boehringer), using the oligonucleotides 'SPETWTNDE' and 'SPETCTHIN', and cloned directionally into the polylinker of pET22B (Novagen) as a 1240 bp *Nde*I/*Hin*dIII restriction fragment. A truncated version of the *petH* gene (Δ*petH*), with a deletion of the first 225 coding nucleotides, was amplified with the oligonucleotides 'SPETTRNDE' and 'SPETCTHIN', and cloned into pET22B, as with the wild-type gene. The *Synechocystis* PCC 6803 *isiB* gene (510 bp), encoding flavodoxin [sll0248; (*30*)], was amplified with the oligonucleotides 'FLANTNDE' and 'FLACTHIN', and cloned into pET22B, as with the *petH* gene.

A truncated version of the *petE* gene, encoding plastocyanin (*31*) lacking the original transit peptide, was amplified with 'PLANTNCO' and 'PLACTECO', and cloned as a 300 bp *Nco*I/*Eco*RI fragment in pET22B. With this construct, translocation of plastocyanin across the plasma membrane of *Escherichia coli* is mediated by the *Erwinia carotovora pelB* (*32*) leader peptide. Cleavage by signal peptidase occurs between residues A22 and A23 in pectate lyase, when expressed in *E. coli* (*32*). Therefore, cleavage of the translocated recombinant plastocyanin fusion protein is predicted to occur between A22 and M23, yielding the N-terminal sequence MANATVK. Cleavage of the transit peptide of native plastocyanin in *Synechocystis* PCC 6803 is proposed to yield the N-terminal sequence NATVK (*31*). Recombinant plasmids were propagated in *E. coli* XLI-Blue and sequenced.

All plasmids, except for the expression construct carrying the wild-type *petH* gene, proved to be unstable in the expression strain *E. coli* BL21[DE3] (Novagen) during induction of the T7 promoter with IPTG. Presumably, excretion of β-lactamase into the culture medium allows a large fraction of the cells in the culture to survive ampicillin concentrations as high as 200 μg/mL without carrying the expression construct. This problem was overcome by intro-

ducing kanamycin resistance into the constructs. The 1.3 kbp *nptII* cassette from pUC4K (Pharmacia), encoding kanamycin resistance, was inserted in the unique *Pst*I site in the β-lactamase gene of pET22B in all plasmids except for the wild-type *petH* expression construct. For the expression construct carrying the *petE* gene, expression levels were approximately 1000-fold increased by this marker exchange.

The Yeast Gal4-Based Two-Hybrid System. The MATCHMAKER Gal4 Two-Hybrid System (Clontech) was used to directly test for interaction between PsaE and PetH. The *psaE* gene was amplified by PCR with the oligonucleotides 'NPSAEXHONDE' and 'CPSAEECOBAM'. The *petH* gene was amplified with the oligonucleotides 'NPETXHONDE' and 'CPETECOBAM'. The PCR products were both digested with *Xho*I and *Eco*RI for cloning into vector pGAD10 (Clontech), and with *Nde*I and *Bam*HI for cloning into vector pAS2 (Clontech), and sequenced. Co-transformants in *Saccharomyces cerevisiae* reporter host strain Y190 (Clontech) were selected on minimal media lacking leucine and tryptophan and histidine, with the addition of 10 mM 3-AT as a competitive inhibitor of the *HIS3* reporter. Co-transformants were sceened for β-galactosidase activity with a colony-lift protocol and X-Gal as the substrate (Clontech).

Oligonucleotides. Oligonucleotide sequences are given from 5′ to 3′. Restriction sites are underlined: 'SPETWTNDE' (forward 5′-GCAATTAACATATGTACAGTCCCGGTAC-3′); 'SPETCTHIN' (backward 5′-CCGCCAAGCTTAGTAGGTTTCCACGTGCCAGC-3′); 'SPETTRNDE' (forward 5′-GCAATTACCATATGCTAGAGGGAGATTCG-3′); 'FLANTNDE' (forward 5′-GCCCACACATATGACAAAAATTGGACTT-3′); 'FLACTHIN' (backward 5′-CGGAAGCTTCTAGGATTGCAAAATTGG-3′); 'PLANTNCO' (forward 5′-CTTCCCGCCATGGCCAATGCAACAGTGAA-3′); 'PLACTECO' (backward 5′-CGACACACGAATTCGGCTGGCTGATTACTC-3′); 'NPSAEXHONDE' (forward 5′-CGCCCTCGAGTTCATATGGCCTTAAATCGTGAC-3′); 'CPSAEECOBAM' (backward 5′-CCGCGGATCCGAATTCCTATTTTGCCGCCGCTTGCAC-3′); 'NPETXHONDE' (forward 5′-CCGCCTCGAGTTCATATGTACAGTCCCGGTTAC-3′); 'CPETECOBAM' (backward 5′-CCGCGGATCCGAATTCCTAGTAGGTTTCCACGTGCCAG-3′).

Expression and Purification of Recombinant Proteins. The recombinant BL21[DE3] *E. coli* strain, carrying the plastocyanin overexpression plasmid, was cultured at 37 °C in a 10 L fermentor with Evans minimal medium (*33*), with 2% (w/v) glucose as a carbon source. Kanamycin (50 μg/mL) and $CuSO_4$ (5 μM) were added to the medium. PetE expression was induced with 1 mM IPTG at an optical density of 2 at 600 nm, and monitored by measuring the absorption at 597 nm of the culture supernatant. To the cell-free culture supernatant were added 20 mM Tris-HCl, pH 8.0, 10 μM $K_3Fe(CN)_6$, and a saturating amount of $(NH_4)_2SO_4$. After 1 h incubation at 4 °C, the precipitated recombinant plastocyanin was pelleted by centrifugation, and desalted either by gel filtration using Sepahadex G-50 or by dialysis against 20 mM Tris-HCl, pH 8.0.

The strains expressing flavodoxin and wild-type or truncated FNR were cultured in a 2 L fermentor, using a phosphate-buffered complex medium, containing 16 g/L tryptone, 10 g/L yeast extract, 5 g/L NaCl, 2.31 g/L KH_2PO_4, and 12.54 g/L K_2HPO_4, with either 50 μg/mL kanamycin (Δ*petH* and *isiB*) or 200 μg/mL ampicillin (wt-*petH*). Expression of the heterologous proteins was induced at $OD_{600} = 2$ with 0.4 mM IPTG. Cells were resuspended in buffer containing 20 mM Tris, pH 8.0, and 0.5 mM PMSF (0 °C), and broken by two passages through a French press (Aminco Corp., USA) at 20 000 psi. The lysate was brought to 1% $(NH_4)_2SO_4$ saturation and centrifuged to remove membrane particles and remaining cell debris. Flavodoxin was reconstituted by incubation of the cell-free extract for 2 h with 50 μM FMN (Sigma) (*34*). Proteins were concentrated by precipitation after the addition of saturated $(NH_4)_2SO_4$, and purified on a Sephadex G-100 FPLC column, equilibrated with a buffer containing 20 mM Tris-HCl, pH 8.0, and 150 mM NaCl. NaCl was subsequently removed, either by dialysis against 20 mM Tris-HCl, pH 8.0, or by gel filtration using Sephadex G-50.

Isolation of Photosynthetic Membranes. Membranes from wild-type *Synechocystis* PCC 6803 and the *psaE* mutant were isolated from cultures grown to high optical density. Cells (2 g wet-weight in 5 mL) were broken in 50 mM Tricine/NaOH, pH 8.0, plus 10 mM NaCl and 0.5 mM PMSF, by three passages through the French press at 20 000 psi (0 °C). The lysate was diluted 5-fold in the same buffer and centrifuged for 15 min at 3000*g* at 4 °C. Membranes were pelleted from the supernatant by ultracentrifugation for 1 h at 41 000 rpm in a Kontron ultracentrifuge (TST4114 rotor; 129000−301500*g*) at 4 °C. The resulting supernatant was discarded, and the pellet was resuspended in the same buffer and recentrifuged in the ultracentrifuge for 1 h. The membranes were finally resuspended in the same buffer at a concentration of approximately 0.5 mg of Chl*a*/mL. Samples used for isolation of PsaE-deficient membranes were also analyzed for complete segregation of the *psaE* deletion by Southern hybridization analysis, as described previously (*17*).

Photoreduction Measurements. Assays of PSI-dependent photoreduction, that are rate-limited at the donor side, were performed in 50 mM Tricine, pH 8.0, 10 mM $MgCl_2$, 0.05% (w/v) *n*-dodecyl β-maltoside, 10 μM DCMU, and photosynthetic membranes (5 μg/mL Chl*a*) (*35*). Methyl viologen (2 mM) was added as the electron acceptor, and 6 mM ascorbic acid together with plastocyanin (1−15 μM) as the electron donor. Oxygen consumption was measured with a Hansatech-type oxygen electrode at 25 °C, with illumination from a 150 W xenon light source, after passing the light through a 350−450 nm band-pass filter. The light intensity was increased until saturation was reached.

Acceptor-side-limited photoreduction assays were performed in 50 mM Tricine, pH 8.0, plus 10 mM $MgCl_2$, 0.05% (w/v) *n*-dodecyl β-maltoside, photosynthetic membranes (5 μg/mL Chl*a*), 6 mM ascorbic acid, 15 μM recombinant plastocyanin, and recombinant FNR (10 nM−1 μM). Recombinant *Synechocystis* PCC 6803 flavodoxin and spinach ferredoxin (Sigma) were used at concentrations of 15 and 5 μM, respectively. $NADP^+$ was added at a concentration of 1 mM. Light from a 150 W xenon lamp was passed through a 650 nm high-pass filter, and used at saturating intensity. NADPH formation was assayed from the increase in absorbance at 340 nm during illumination, using a Model HP 8453 Hewlett-Packard diode array spectrophotometer (Portland, OR).

Kinetic Simulations. A kinetic model was constructed in order to simulate light-driven electron transport from reduced

Table 1: Light-Driven PSI-Mediated Electron-Transport Rates with Various Electron Donors[a]

electron donor (concn)	O_2 consumption rate [μmol of O_2·(mg of Chl*a*)$^{-1}$·h^{-1}]	calcd turnover no. (e^-·PSI^{-1}·s^{-1})[b]
DCPIP (0.1 mM)	380	14.1
DAD (0.1 mM)	127	4.8
TMPD (0.1 mM)	271	10.2
horse heart cyt *c* (50 μM)	304	11.1
rec. plastocyanin (15 μM)	2702	100.7

[a] Rates are determined by O_2 uptake measurements, mediated by F_B-reduced methyl viologen. [b] A Chl*a*:P700 ratio of 150:1 is assumed for thylakoid membranes.

plastocyanin to $NADP^+$ with the Gepasi Bio/chemical Kinetics Simulator software package version 3.1 (*36*). All reaction constants were introduced as reversible bimolecular second-order rate constants, or reversible first-order rate constants, taken from the literature and from this work. Moiety conserved relations were calculated using the Gepasi package. Response coefficients (*R*) were calculated from the enzyme concentration (*E*) dependent change in flux (*J*) according to: $R_E^J = (\delta J/J)/(\delta E/E)$.

RESULTS

Production and Purification of Recombinant Electron Transport Proteins. The sequence of the genes encoding *Synechocystis* PCC 6803 flavodoxin, plastocyanin, and FNR has been published (*29*−*31*), allowing the design of oligonucleotides to be used for amplification of these genes, for in-frame insertion into the overexpression plasmid pET22B. Heterologous expression of the complete *petE* gene in *E. coli* leads to the accumulation of the PetE protein in the periplasm (*28*). However, replacing the endogenous transit peptide of plastocyanin with the *Erwinia carotovora pelB* leader peptide resulted in the accumulation of the recombinant electron carrier in the culture supernatant at levels as high as 40 mg/L, coloring the culture supernatant distinctly blue−green. Cytoplasmic expression of wild-type and truncated FNR, and of flavodoxin, yielded recombinant products that were accumulated at levels of 20−50% of soluble cytoplasmic protein.

Recombinant Plastocyanin Is the Superior Electron Donor to Photosystem I. To study electron transport at the acceptor side of PSI, it is necessary to make the acceptor-side reactions rate-limiting for the overall reaction of electron transfer from ascorbic acid to $NADP^+$. This is achieved by supplying a relatively high concentration of reduced electron carriers that reduce the $P700^+$ cation at a faster rate than F_B^- can be oxidized. Donor-side-limited photoreduction assays in the presence of methyl viologen show that artificial electron donors do not meet this requirement, whereas recombinant plastocyanin catalyzes high rates of electron transport (Table 1).

Plastocyanin was therefore titrated between 1 and 15 μM concentration in these assays, to determine the K_m for plastocyanin in this reaction. With a fixed concentration of PSI reaction centers, Michaelis−Menten kinetics were observed with a K_m value of 7.0 μM and a V_{max} of approximately 3531 μmol of O_2·(mg of Chl*a*)$^{-1}$·h^{-1}, corresponding to a calculated turnover number of 132 e^-·PSI^{-1}·s^{-1}. From the slope of the double-reciprocal plot of the rate versus the plastocyanin concentration, a second-order rate constant is estimated of 1.88×10^7 M^{-1}·s^{-1}, with a corresponding off-rate of 132 s^{-1} for the plastocyanin/PSI complex. This value is in reasonable agreement with the experimentally determined value at pH 7.5 and low ionic strength for *Synechocystis* PCC 6803 plastocyanin and PSI, i.e., 8.6×10^6 M^{-1}·s^{-1} (*37*). It has been proposed that the reaction between *Synechocystis* plastocyanin and PSI does not involve the formation of an intermediate complex, as is the case for spinach plastocyanin and PSI, but follows a 'simple oriented collisional mechanism', resulting in a monophasic reduction of P700 (*38*).

Table 2: Photoreduction Activites of Wild-Type- and PsaE-Deficient Photosynthetic Membranes[a]

thylakoids	donor-side-limited rate[b] PC (15 μM) → MV	acceptor-side-limited rate[c] PC (15 μM) → $NADP^+$	
		WT FNR (100 nM)	trunc. FNR (100 nM)
WT	2702	387 ± 26	462 ± 27
PsaE$^-$	2571	148 ± 25	242 ± 40

[a] Light-dependent, methyl viologen mediated, O_2 uptake activities and $NADP^+$ photoreduction activities were measured using 15 μM plastocyanin. This concentration catalyzed near-maximal turnover numbers of PSI. Spinach ferredoxin (included at 5 μM) was used in combination with either recombinant wild type or truncated FNR (100 nM) for the $NADP^+$ photoreduction measurements. [b] Micromoles of O_2 per milligram of Chl*a* per hour. [c] Micromoles of NADPH per milligram of Chl*a* per hour.

Acceptor-Side-Limited Photoreduction Rates Are Decreased in PsaE-Deficient Thylakoids of Synechocystis PCC 6803. We observed that PsaE-deficient thylakoids displayed activity in donor-side-limited photoreduction assays almost equal to wild-type membranes [2571 μmol of O_2·(mg of Chl*a*)$^{-1}$·h^{-1} versus 2702 μmol of O_2·(mg of Chl*a*)$^{-1}$·h^{-1} for the wild type], when using 15 μM plastocyanin (Table 2). Fluorescence emission spectra obtained with 440 nm excitation, taken at 77 K, of these thylakoids indicate a slightly decreased PSI/PSII ratio for the mutant membranes, providing a possible explanation for the somewhat decreased activity of the PsaE-deficient thylakoid membranes (not shown).

In acceptor-side-limited photoreduction assays, using fixed concentrations of electron carriers, a decreased activity was measured with PsaE-deficient thylakoids compared to wild-type thylakoids (Table 2). Possibly a somewhat higher activity was observed when truncated 38 kDa FNR was used at a concentration of 100 nM, when compared to assays including wild-type 47 kDa FNR (Table 2). This was tested to determine if the positively charged N-terminal domain of wild-type FNR, that is homologous to the 9 kDa CpcD phycobilisome linker polypeptide, influences the photoreduction kinetics. However, a small deviation from the quantified FNR concentration can result in the observed difference in photoreduction activities. Therefore, within the accuracy of the obtained data, no possible contribution of the N-terminal domain was apparent in the wild type, nor in the *psaE* mutant. In addition, no significant difference for both wild-type- and PsaE-deficient membranes was observed when spinach ferredoxin (5 μM) was replaced by *Synechocystis* PCC 6803 flavodoxin (15 μM) either (not shown).

FNR Still Has Control over the Rate of $NADP^+$ Photoreduction at 750 nM Concentration in the Case of PsaE-

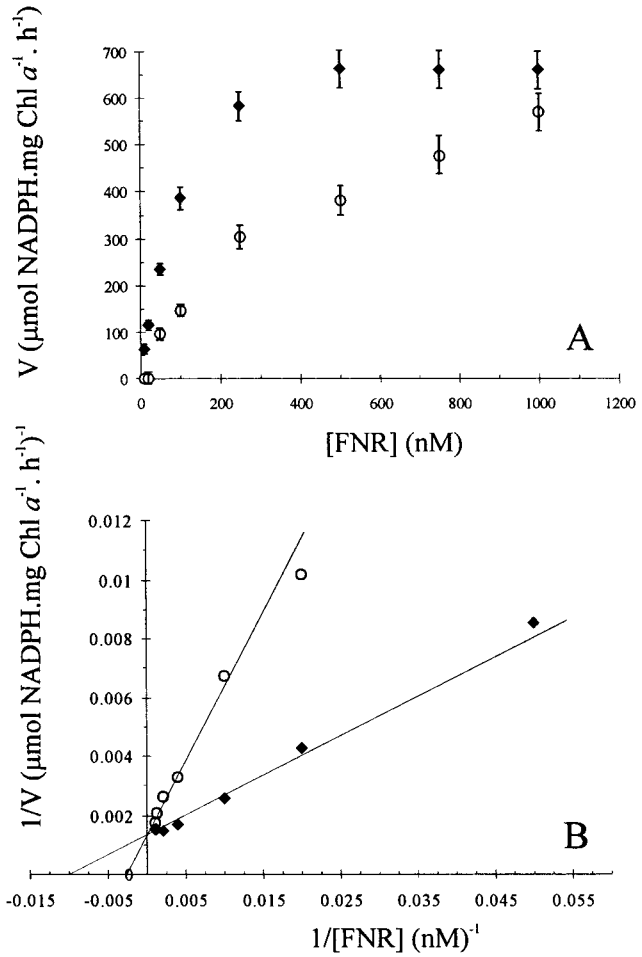

FIGURE 1: $NADP^+$ photoreduction rates of wild-type- and PsaE-deficient membranes with varying concentrations of wild-type 47 kDa FNR (A) Activities of $NADP^+$ photoreduction were determined. Concentrations of plastocyanin, Chl*a*, ferredoxin, and $NADP^+$ were the same as in Table 2. Error bars represent the standard deviations for the measurements. Filled diamonds (◆) present the measurements with wild-type thylakoid membranes; open circles (○) present the measurements with PsaE-deficient membranes. (B) Double reciprocal plot of the $NADP^+$ photoreduction activities.

Deficient Thylakoids, in Contrast to Wild-Type Thylakoids. The concentrations of ferredoxin (5 μM) and flavodoxin (15 μM) used in the acceptor-side-limited photoreduction assays were found to be saturating for the observed rates. Titrations of wild-type 47 kDa FNR in these assays revealed saturation behavior for the FNR-dependent rate of electron transport (Figure 1).

At a concentration of 100 nM FNR, the $NADP^+$ photoreduction activity of PsaE-deficient membranes was significantly lower than rates obtained with wild-type PSI. This was observed both with ferredoxin and flavodoxin, and with wild-type as well as truncated FNR (Table 2). In contrast to the observed rates with wild-type membranes, $NADP^+$ photoreduction rates increased with increasing concentrations of FNR above 500 nM when PsaE-deficient membranes were used (Figure 1). At a concentration of 500 nM, the $NADP^+$ photoreduction rate with wild-type membranes was 49 (±6)% of the donor-side-limited rate, comparable to the rate with 1 μM FNR. In contrast, the rate with PsaE-deficient membranes increased from 30 (±4)% of the donor-side-limited rate at 500 nM FNR to 44 (±6)% at 1 μM FNR.

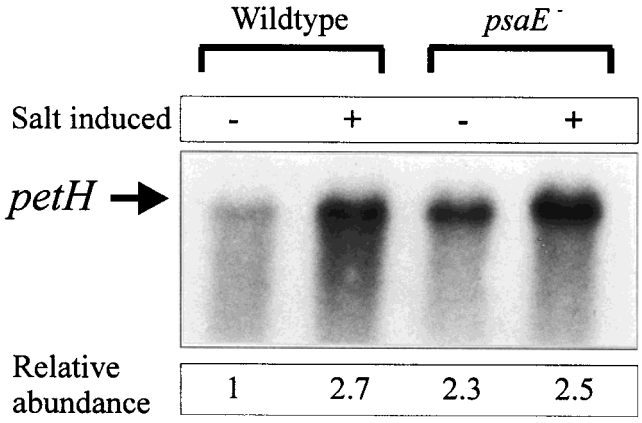

FIGURE 2: Expression levels of *petH* mRNA in the wild-type and *psaE* mutant. Lane 1, wild-type cells grown photoautotrophically. Lane 2, wild-type cells upon salt stress. Lane 3, *psaE* mutant cells grown photoautotrophically. Lane 4, *psaE* mutant cells upon salt stress. For details, see Materials and Methods.

Thus, at 1 μM concentration of FNR, the rates of $NADP^+$ photoreduction were no longer significantly different between wild-type- and PsaE-deficient membranes. For both the wild-type- and the PsaE-deficient membranes, the maximal extrapolated rates of $NADP^+$ photoreduction were approximately 60% of the donor-side-limited rates (using either exponential or Michaelis−Menten kinetics to fit the data). Figure 1B presents a double reciprocal plot of the data, indicating that most likely a change in the affinity for FNR of the reconstituted photoreduction system is the origin of the reduced activities observed in acceptor-side-limited assays with relatively low concentrations of FNR. However, from these data, it cannot be judged if the kinetics follow Michaelis−Menten saturation behavior. In the case of wild-type PSI, about 105 nM wild-type FNR catalyzes 50% of the maximal rate, whereas 397 nM FNR is required to catalyze approximately 50% of the maximal rate in the case of PsaE-deficient PSI.

Thus, the deficiency in the linear electron transport capacity of the *psaE* mutant can be compensated by increasing the concentration of FNR in the in vitro assays. This is in line with the experimental observation that the yield of ferredoxin reduction by PsaE-deficient PSI is equal to that of the wild type (*17*), implying that the maximal rate of electron transport through plastocyanin, PSI, and ferredoxin should be the same.

Expression of petH Is Increased in the psaE Mutant. It has been reported earlier that the growth rate under photoautotrophic conditions of the *Synechocystis* PCC 6803 *psaE* mutant is not significantly different from that of the wild type (*16*). The same was observed in the comparison of the *Synechococcus* PCC 7002 *psaE* mutant with the wild-type strain (*39*). This suggests that oxygenic linear electron transport, involving both PSII and PSI, in the *psaE* mutant proceeds with an efficiency close to the wild-type level. We therefore assayed the mRNA level of *petH*, encoding ferredoxin−$NADP^+$ reductase, in the wild-type and in the *psaE* mutant in standard autotrophic growth conditions (at a light intensity of 70 $\mu E \cdot m^{-2} \cdot s^{-1}$), as well as in a salt-stressed culture. During salt stress (applied via the addition of 0.5 M NaCl to the growth medium) of a culture of *Synechocystis* PCC 6803, increased abundance of the *petH* mRNA was observed earlier (*29*). The Northern blot shown in Figure 2

demonstrates that the *petH* expression level in the *psaE* mutant is elevated, relative to the expression level in the wild type, when cells are grown under standard photoautotrophic conditions, whereas in salt-stressed cultures the *petH* mRNA levels are comparable in the wild type and the mutant. Presumably, the increase in the accumulated level of mRNA results from induction of the stress promoter that regulates *petH* expression (*29*). Higher concentrations of *petH* mRNA were accompanied by an increase in the enzyme activity that was subsequently determined in cell-free extracts (*29*). This was also confirmed in the case of the *psaE* mutant: the enzyme activity is approximately twice as high in the mutant as in the wild type, when expressed on the basis of the amount of Chl*a* (not shown). It is proposed that the increased level of FNR in the *psaE* mutant compensates for the decreased rate of linear electron transport, as in the in vitro assays.

A Kinetic Model of Light-Driven, PSI-Dependent Linear Electron Transport from Reduced Plastocyanin to NADP$^+$. The observation that deletion of subunit PsaE from PSI results in an altered FNR saturation profile for the NADP$^+$ photoreduction assays is not easily understood in terms of ferredoxin photoreduction kinetics. PsaE-deficient PSI reaction centers are partially deficient in ferredoxin reduction (*22*). To predict wether the mutationally induced changes will affect the linear electron-transfer capacity of the reaction centers, and, if so, how, a kinetic model was constructed that incorporates all partial reactions from reduced plastocyanin to NADP$^+$. All reaction rate constants were introduced as reversible first-order and bimolecular second-order rate constants that were taken either from the literature or from this work (Figure 3).

First, electron donation by plastocyanin to PSI was modeled and tested for turnover numbers at relevant concentrations of the reactants. Then, ferredoxin reduction was added to the model, using the reaction constants published for *Synechocystis* PCC 6803 PSI and spinach ferredoxin. Separately, reduction of NADP$^+$ by FNR in the presence of reduced ferredoxin was modeled, and tested for turnover numbers and, specifically, inhibition by oxidized ferredoxin. Finally, all reaction rate constants were used to model the complete set of reactions for electron transfer from reduced plastocyanin to NADP$^+$, and tested for the pre-steady-state kinetics, overall turnover numers, and concentration of intermediates that accumulate in the steady state.

The NADP$^+$ photoreduction assay consists of several electron-transfer steps, which require the formation of several transient complexes. First, P700$^+$ is rereduced by plastocyanin. Since this reaction in *Synechocystis* is believed to follow a collisional reaction scheme (*38*), it can be described in terms of a second-order rate constant and an off-rate that is calculated from the apparent K_m in acceptor-side rate-limited photoreduction assays. This approach uses the assumption that at the concentration of reactants used, the rate of the overall reaction is limited by the second-order rate constant, instead of the first-order electron-transfer kinetics. When this holds, the K_m value determined for this system can be taken as the value for K_d. The complete set of reactions on which the photoreduction assay is based is given in Figure 3.

Assuming the same affinity for reduced as for oxidized plastocyanin, it was necessary to implement a somewhat higher second-order rate constant (1.88×10^7 M^{-1}•s^{-1}, with a K_d of 7.0 μM) than determined previously (*37*) (Figure 3). Note that the turnover of PSI at high concentrations of plastocyanin becomes limited by, and is therefore equal to, the concentration-independent off-rate for the plastocyanin/PSI complex. This part of the model, together with the introduction of an artificial electron sink, to simulate the effect of illumination, was sufficient to accurately simulate the Michaelis−Menten-like plastocyanin saturation kinetics that were determined experimentally. In particular, the simulated turnover number of PSI with 15 μM plastocyanin is identical (not shown) to the measured value (Table 1).

With the introduction of a fixed concentration of 5 μM oxidized ferredoxin, the initial PSI turnover numbers are almost equal to turnover numbers in the donor-side-limited assays, due to the very high second-order rate constant for ferredoxin and PSI (Figure 3). For the model, a simplification is introduced by assuming the same binding kinetics for oxidized as for reduced ferredoxin. The second-order rate constant and K_d for *Synechocystis* PSI and spinach ferredoxin were taken from (*40*).

The catalytic activity of FNR, presumably, is limited by the dissociation of oxidized ferredoxin under conditions where the maximal turnover is measured (*41*). FNR is reduced by ferredoxin twice, to yield the semiquinone [FNR(sq)] and the fully reduced [FNR(red)] species, respectively, before NADP$^+$ is reduced to NADPH (*41*). NADP$^+$ is bound by FNR in the oxidized state, so that a ternary complex, NADP$^+$/FNR/ferredoxin, is formed, intermediate in the catalytic cycle. Indeed, formation of the FNR/NADP$^+$ complex was found to be too fast to determine with stopped-flow experiments (*42*). The kinetic model is therefore simplified by neglecting the binding and dissociation of the oxidized and reduced nucleotide, respectively, by FNR, and accounts only for the interactions of FNR with ferredoxin. Competitive inhibition of binding of reduced ferredoxin to FNR, by oxidized ferredoxin, however, is explicitly included (Figure 3).

The model for ferredoxin:NADP$^+$ oxidoreductase was tested for the turnover numbers that would be obtained. For the *Spirulina platensis* ferredoxin and FNR, it was found experimentally that in the presence of NADP$^+$ and with a high Fd(red):Fd(ox) ratio [i.e., in the absence of competitive inhibition by Fd(ox)], a steady-state turnover number of 729 e$^-$ s^{-1} could be reached at 20 °C (*43*). The kinetic model predicts a maximal turnover number of 103 (NADPH) s^{-1} (206 e$^-$ s^{-1}) in the absence of oxidized ferredoxin. Clearly, the kinetics during turnover are faster than what is calculated from the K_d values and the second-order rate constants. In particular, the off-rates are expected to be higher than the predicted values. For instance, when the off-rate for oxidized ferredoxin is increased to 1000 s^{-1}, a maximal turnover of 170 (NADPH) s^{-1} (340 e$^-$ s^{-1}) is calculated. Increasing the second-order rate constant for both oxidized and reduced ferredoxin to 5×10^8 M^{-1}•s^{-1}, and using an off-rate of 1100 s^{-1} (K_d value unchanged), increases the maximal turnover to 470 (NADPH) s^{-1} (940 e$^-$ s^{-1}). These examples indicate that during turnover of the catalytic cycle of FNR the off-rates for oxidized ferredoxin must be higher than the off-rates that are calculated from the dissociation constants and the second-order rate constants for the oxidized and reduced species of ferredoxin and FNR. This would explain the high turnover number that is observed in vitro (*43*).

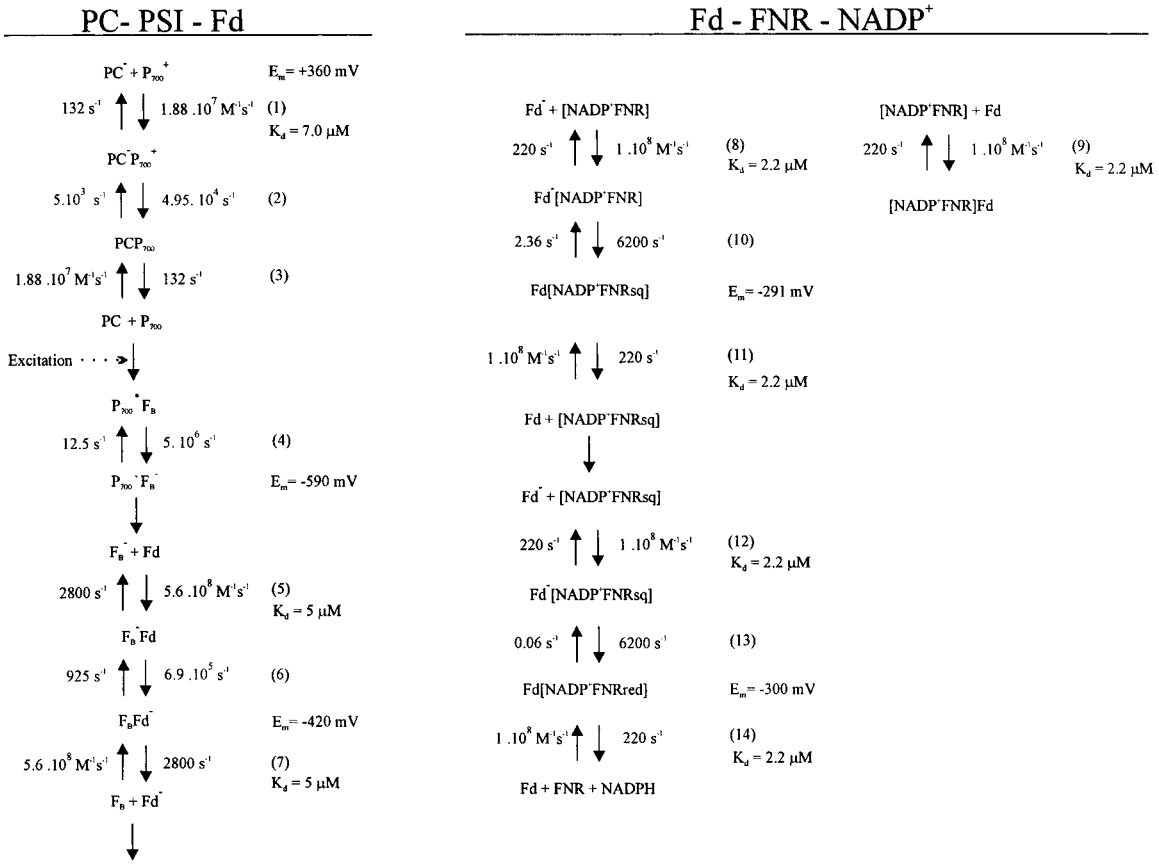

FIGURE 3: Reaction constants involved in PSI-dependent linear electron transport from plastocyanin to $NADP^+$. (1) The second-order rate constant for the reaction between recombinant *Synechocystis* plastocyanin and *Synechocystis* PSI was determined in this study, and is comparable to the value determined previously (*37*). The off-rate is calculated from the dissociation constant (7.0 μM), as experimentally determined for this system. (2) The fastest phase of $P700^+$ reduction, reflecting k_{et}, was determined with a $t_{1/2}$ of 14 μs for spinach plastocyanin and PSI (*44*). The rate of the backward reaction is calculated using the Nernst equation, considering the midpoint potential that was determined for *Synechocystis* PCC 6803 plastocyanin specifically (*45*). (3) Assuming the same dissociation constant for reduced as for oxidized plastocyanin. (4) Both F_A and F_B are reduced by F_X in approximately 200 ns after excitation of P700. The back-reaction from F_B to F_X proceeds with a time constant of approximately 80 ms (*46*). Although it is not known if either $F_A$or F_B or both F_A and F_B act as electron donor to ferredoxin, recent studies implicate F_B as the direct donor (*46*, *47*). The kinetics of the fast electron-transfer steps in the reaction center are neglected and considered to be reversible, including the charge separation event. (5) Laser flash induced ferredoxin reduction at high protein concentration allowed the determination of the second-order reaction constant for the *Synechocystis* PCC 6803 photosystem I/spinach ferredoxin couple, due to the relatively high K_d (5 μM) (*40*). In the case of the *psaE* mutant, these values are replaced by 2.8×10^8 $M^{-1}\cdot s^{-1}$ and $K_d = 500$ μM; $k_{off} = 1.4 \times 10^5$ s^{-1}, according to Barth et al. (*22*) (see Results). (6) Several first-order phases of ferredoxin reduction are observed at high protein concentrations. In the case of the *Synechocystis* PCC 6803 photosystem I/spinach ferredoxin couple, two phases were measured, with half-lives of 1 and 5 μs (*40*). The rate of the back-reaction was calculated using the Nerst equation, considering only the midpoint potential of F_B. (7) Assuming the same dissociation constant for reduced as for oxidized ferredoxin. In case of the *psaE* mutant, see also step (5). (8) The second-order reaction constant for reduced ferredoxin and FNR was determined for several systems (*48*−*50*). The binding constants are strongly dependent upon salt concentration. Contributions of hydrophobic interactions at high ionic strength (100 mM) and electrostatic interactions at low ionic strength (12 mM) are implicated (*50*). At low ionic strength, ferredoxin-mediated reduction is independent of the presence of the CpcD-homologous N-terminal domain of *Synechocystis* PCC 6803 FNR (Table 2), and *Anabaena* PCC 7119 FNR (*51*). A dissociation constant for reduced Fd of 2.2 μM and a second-order rate constant of 1×10^8 $M^{-1}\cdot s^{-1}$ are taken from the *Anabaena* PCC 7119 Fd and native FNR (*50*). Reduced Fd binds FNR, forming a ternary complex together with $NADP^+$ (*41*). (9) At low ionic strength, a [Fd(ox)FNR(ox)] complex is formed within the 'dead-time' of a stopped-flow experiment [second-order rate constant $> 1 \times 10^8$ $M^{-1}\cdot s^{-1}$ and $K_d < 0.1$ μM (in the absence of $NADP^+$) for spinach Fd and FNR; (*52*)]. Thus, oxidized ferredoxin is a competitive inhibitor during forward electron transport. A K_i of 2.2 μM was calculated for oxidized Fd in a steady-state experiment involving *Spirulina platensis* Fd and FNR (in the presence of $NADP^+$) (*43*). For *Anabaena* PCC 7119 Fd and FNR, a K_d for Fd(ox) of <1 μM was estimated from the inhibitory effect of a [Fd(ox)FNR(ox)] complex in flash photolysis studies of FNR reduction by photoreduction of Fd with EDTA/5-deazariboflavin (*50*, *53*). The K_i determined for *Spirulina platensis* Fd(ox) and FNR(ox) (*43*) is taken as a value for K_d, since it is determined during steady-state electron transport in the presence of $NADP^+$. In addition, *Spirulina* FNR shows the highest homology of all known sequences to the *Synechocystis* PCC 6803 FNR (*29*). (10) With the use of flash photolysis studies, the first-order rate constant reflecting forward electron transport from *Anabaena* PCC 7119 Fd to FNR was 6200 s^{-1} (*54*). The calculated rate for the back-reaction, assuming a potential for Fd-bound FNR(sq) of −291 mV (*54*) and the potential of spinach Fd shifted to −450 mV due to FNR binding (*55*), would become 0.08 s^{-1}. However, the experimentally determined value was 2.36 s^{-1} (*56*). (11) Assuming the same binding kinetics of Fd(ox) for FNR(ox) and FNR(sq). (12) Assuming the same rate of reduction for FNR(sq) as for FNR(ox) by Fd(red). The calculated rate for the back-reaction, assuming a potential of −300 mV for the FNR(sq)/FNR(red) couple, is 0.06 s^{-1}. (13) Assuming the same binding kinetics of Fd(ox) for FNR(ox) as with the ternary complex together with $NADP^+$.

However, the turnover number of FNR during PSI-dependent linear electron transport from plastocyanin to $NADP^+$ is lower than the maximal rates that were determined by Masaki et al. (*43*) and Batie and Kamin (*41*). The simulations predict that there is no influence of the off-rate within the range from 220 to 1100 s^{-1} on the maximal (with

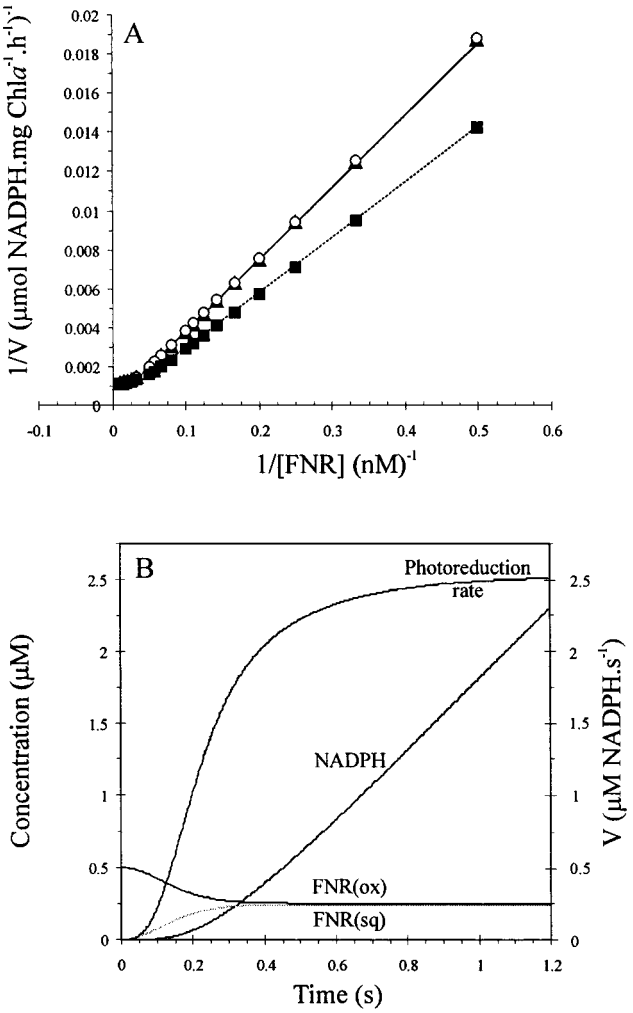

FIGURE 4: Simulation of PSI-dependent linear electron transport. (A) Double reciprocal plot of the FNR-dependent rates of NADPH formation reached in steady state. (▲) 'Wildtype' series, calculated using the kinetic data given in Figure 3, whereas the (○) 'PsaE' dataset represents the simulated results obtained with the modified ferredoxin reduction kinetics obtained for the *psaE* mutant [2.8×10^8 $M^{-1}\cdot s^{-1}$ and $K_d = 500$ μM; $k_{off} = 1.4 \times 10^5$ s^{-1}; (*22*)]. The (■) 'Complex' series (referring to the ternary complex PSI/Fd/FNR) refers to the case with an increased second-order rate constant for both oxidized and reduced ferredoxin and FNR (5×10^8 $M^{-1}\cdot s^{-1}$). Plastocyanin is included at 15 μM concentration, and PSI at 75 nM concentration (10 μg of Chl *a*/mL). (B) Simulated transient concentrations of NADPH, FNR(ox), and FNR(sq) and rate of $NADP^+$ photoreduction (micromolar NADPH formed per second with given concentrations of reactants). FNR is initially included at 500 nM concentration in the oxidized state. Kinetic constants and concentrations were as in Figures 3 and 4A (WT). The steady-state accumulation of the oxidized and semiquinone species of FNR represents the fastest proces in the simulation with the given concentrations of reactants.

saturating FNR concentration) overall flux through the system. The saturation characteristics for FNR are altered only when the off-rate decreases below 50−80 s^{-1}, but remain sensitive to the second-order rate constant between ferredoxin and FNR.

Using the kinetic constants given in Figure 3, a strong dependence of the concentration of FNR on the rate of NADPH formation is predicted by the model at nanomolar concentrations of FNR (Figure 4A). The simulations show that the saturation kinetics of FNR for the overall rate are not Michaelis−Menten kinetics. In particular, a deviation from Michaelis−Menten kinetics is observed at higher concentrations of FNR (Figure 4A). At low concentrations of FNR, the saturation kinetics more resemble Michaelis−Menten kinetics. A true K_m (Michaelis−Menten) value is therefore not extracted from the model; rather a value is taken from the *v*/[FNR] curves, representing the concentration of FNR that catalyzes 50% of the maximal rate. Using the second-order rate constants for ferredoxin and FNR as shown in Figure 3, it is simulated that 20 nM FNR catalyzes 50% of the maximal rate. At high concentrations of FNR (>1 μM), inhibition of the flux is observed. This is due to complexation of oxidized ferredoxin by FNR when the former is added in excess over ferredoxin: it was predicted that the steady-state overall flux through the system is dependent on the concentration of free oxidized ferredoxin. At low concentration, the control of FNR over the total flux is very high (a response coefficient of $R = 0.98$ was estimated at 5 nM concentration; derived from the 'WT' dataset presented in Figure 4A), but this control becomes lower at higher concentrations (response coefficient of $R = 0.02$ at 500 nM). Due to inhibition by depletion of free oxidized ferredoxin, at high concentrations the control of FNR even becomes negative (response coefficient of $R = -0.04$ at 5 μM).

The kinetic simulation predicts that at 500 nM FNR the flux through the system reaches a steady state after approximately 1200 ms, whereas the oxidized and semiquinone species of FNR reach steady-state levels in 400 ms (Figure 4B). All free and complexed species of the oxidized and semiquinone states of FNR were summed for these calculations. Therefore, all states that are spectroscopically visible are accounted for. During turnover, it was experimentally determined for spinach ferredoxin and FNR that approximately 50% of the fully oxidized state and approximately 40% of the semiquinone state accumulate (*41*). This observation was actually used as an argument that dissociation of oxidized ferredoxin is important as a rate-liming step in the catalytic cycle. The time it takes for these species of FNR to accumulate to steady-state levels is a function of the FNR:PSI ratio. Both the concentration of FNR and the apparent turnover number of FNR will determine the time that is required for steady-state formation.

Given a fixed concentration of PSI reaction centers, the oxidized and semiquinone species of FNR accumulate to 50% levels much faster, at low concentrations of FNR, whereas the steady state for NADPH formation is reached later. At low concentrations, when FNR has a high control, the simulated turnover number in steady state is relatively high (148 e^- s^{-1} at 5 nM), although still not high enough to expect an effect of modifications of the affinities of FNR for reduced and oxidized ferredoxin, as presented in Figure 3. At 500 nM, the calculated turnover number has become 10.7 e^- s^{-1}, and it has dropped to 1.06 e^- s^{-1} at 5 μM.

The kinetic simulations predict that the highest $NADP^+$ photoreduction activity that is reached with a saturating concentration of FNR is close to 970 μmol of NADPH·(mg of Chl*a*)$^{-1}$·h^{-1} (72% of donor-side-limited rate). In fact, at high concentrations of FNR, electron donation to $P700^+$ gains control over the flux. The highest rates that were determined experimentally [up to 650 μmol of NADPH·(mg of Chl*a*)$^{-1}$·h^{-1}; Figure 1] still do not reach this value. Since the affinity of the *Synechocystis* PCC 6803 FNR/spinach

ferredoxin couple is not known, it is difficult to predict the concentration of FNR that catalyzes the maximum rate, and the concentration where inhibition due to complexation of oxidized ferredoxin becomes significant. In addition, direct reduction of oxygen by the reduced Fe-S clusters of PSI and/or ferredoxin may be a competing side-reaction that occurs during in vitro $NADP^+$ photoreduction assays, when these are performed under aerobic conditions. The rate at which this reaction occurred has not been determined experimentally, and may have decreased the maximal rate of $NADP^+$ reduction. It should also be mentioned that it is inherent to this system that the concentration of FNR that catalyzes 50% of the maximal rate is influenced by the rate at wich $P700^+$ is maximally reduced by electron donors: decreasing the second-order rate constant for plastocyanin and PSI to 6.4×10^6 $M^{-1}\cdot s^{-1}$ (with the same $K_d = 7.0$ μM) shifts this calculated concentration from 20 to 8 nM FNR. Including near-saturating concentrations of plastocyanin in our assays has therefore ensured that the highest value possible was measured experimentally. On the other hand, it explains why low concentrations of FNR can be saturating if artificial electron donors such as DCPIP are used, that show much lower rates of reduction of $P700^+$ (Table 1).

The Reduced Affinity of PsaE-Deficient PSI for Ferredoxin Is Predicted Not To Influence the Linear Electron-Transport Capacity. It was previously indicated that deletion of PsaE results in partially deficient ferredoxin reduction (*17*). An important observation was that a high yield of ferredoxin reduction was determined, for PsaE-deficient reaction centers, by measuring the $P700^+F_B^-$ recombination rate in the presence and in the absence of ferredoxin, indicating that under conditions where electron donation to PSI is fast the deficiency at the acceptor side of the mutant is compensated in terms of turnover rates (*17*). The influence of the mutation on the kinetics of ferredoxin reduction was accurately determined recently (*22*). It appears that for *Synechocystis* PCC 6803 ferredoxin and PSI a relatively small decrease of the second-order rate constant for ferredoxin and PSI (factor of 2), but a large increase in the dissociation constant (factor of 100), results from the absence of the stromal subunit PsaE (*22*).

These numbers were determined for wild type and $PsaE^-$ *Synechocystis* PSI and ferredoxin [K_ds 0.5 and 52 μM, respectively; (*22*)]. These observations were implemented into the model, assuming that with spinach, instead of *Synechocystis*, ferredoxin the same increase in the dissociation constant for the PSI/ferredoxin complex results from the deletion of *psaE*. A model for the *Synechocystis* PCC 6803 PsaE-deficient PSI and spinach ferredoxin was tested, using a second-order rate constant of 2.8×10^8 $M^{-1}\cdot s^{-1}$ and a k_{off} value of 1.4×10^5 s^{-1} for both oxidized and reduced ferredoxin and PSI ($K_d = 500$ μM). The resulting turnover number of the system is predicted not to be affected by these changes. In addition, the calculated saturation profile for FNR is almost identical, when these numbers are used (Figure 4A). The rate of dissociation of the PSI/Fd complex is in the range where it can compete with the rate of ferredoxin reduction (Figure 3). However, the forward electron-transport rate exceeds the rate of complex dissociation approximately 5-fold, explaining the lack of effect on the overall electron-transport kinetics (Figure 4A). That this is also the case during experimental conditions is reflected by the maximal rate that was determined for PsaE-deficient membranes, in addition to the high ferredoxin reduction yield (*17*). These calculations indicate that the effects of the *psaE* mutation on the ferredoxin reduction kinetics do not explain the observed effects on the FNR saturation profile (Figure 1).

The Ternary Complex PSI/Ferredoxin/FNR Must Be Assumed in Order To Simulate a Decrease of the Concentration of FNR That Catalyzes Half the Maximal Rate of $NADP^+$ Photoreduction. The affinity of FNR for ferredoxin is important for the saturation kinetics of the system. Changing the affinity of FNR for ferredoxin results in altered values for the concentration of FNR that catalyzes 50% of the maximal rate, according to the simulations. In particular, the second-order rate constant for FNR and ferredoxin determines the shape of the υ/[FNR] saturation curve. The maximal rate that is reached is not a function of this parameter within the limits that were tested with the model (1×10^5 $M^{-1}\cdot s^{-1}$–5×10^8 $M^{-1}\cdot s^{-1}$). The off-rate for the ferredoxin/FNR complex does not greatly influence the shape of the saturation curve, as long as it does not decrease below 50–80 s^{-1}, which is not expected from the literature data (Figure 2). An increase in the second-order rate constant (for both reduced and oxidized ferredoxin) was found to simulate a decrease in the apparent affinity the photoreduction system for FNR. When a value of 5×10^8 $M^{-1}\cdot s^{-1}$ was tested, the maximal rate through the system was not affected, but the concentration of FNR that catalyzed 50% of the maximal rate was 13 nM (Figure 4A; 'Complex' series).

Thus, the kinetic behavior that is the result of a mutation of PSI is most likely explained by assuming a modification of the affinity of FNR for ferredoxin. The most straightforward explanation for the experimental results is to assume the formation of a PsaE-dependent transient ternary complex, PSI/ferredoxin/FNR (Figure 5). Such a transient complex can be modeled by increasing the affinity of FNR for ferredoxin, by increasing the corresponding second-order rate constant. This would explain why a mutation in PSI can influence the apparent affinity of FNR for ferredoxin. The observed saturation profile of the PsaE-deficient photosynthetic membranes could be simulated using a second-order rate constant of 1.5×10^6 $M^{-1}\cdot s^{-1}$, whereas the saturation profile of the wild-type could be simulated using a value of 6.8×10^6 $M^{-1}\cdot s^{-1}$. The postulated ternary complex therefore increases the affinity by a factor of approximately 4.5. The resulting K_d values (taking the minimal value for the off-rate of 50 s^{-1}) then become 33 and 7 μM, respectively. Certainly, these values are higher than the measured constants for 'homologous' systems (such as spinach ferredoxin/FNR; Figure 3). Probably a low affinity in these experiments is due to the non-native couple spinach ferredoxin and *Synechocystis* PCC 6803 FNR. The association between these two electron carriers is strongly dependent on ionic strength, and is perhaps not optimal under our experimental conditions.

In fact, native systems seem to behave as predicted by the simulations based on the numbers shown in Figure 3. Using spinach chloroplasts, 40 nM spinach FNR was found to catalyze 50% of the maximal rate of $NADP^+$ photoreduction (*57*). $NADP^+$ photoreduction rates for *Anabaena variabilis* 7120 PSI and ferredoxin can give high activities at low concentrations: the turnover number determined for FNR in the $NADP^+$ photoreduction assay at 8.2 nM concentration was already 101 s^{-1} (recombinant full-length

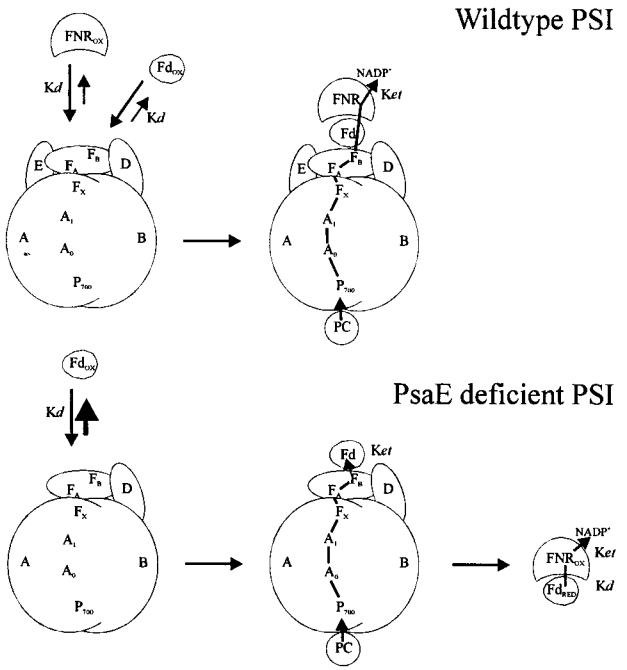

FIGURE 5: Model for the formation of a PsaE-dependent transient ternary complex between PSI, ferredoxin, and FNR wild-type PSI recruits both ferredoxin and FNR in a transient fashion, and electron transport proceeds within the lifetime of the complex. In the case of PsaE-minus PSI, ferredoxin is bound and reduced by PSI, dissociates, and complexes with FNR. The thick arrow indicates the increased off-rate for the ferredoxin/PSI complex [according to Barth et al. (*22*)].

Anabaena FNR) or 77 s^{-1} (native 36 kDa *Anabaena* FNR) (*51*). The low FNR concentration that was used in these assays demonstrated the high affinity between FNR and ferredoxin for these native couples. The high turnover numbers are probably due to a high ratio of reduced vs oxidized ferredoxin in steady-state conditions, since PSI was added at high concentrations. This effect can be simulated with our kinetic model as well.

In this respect, it is interesting to note the $NADP^+$ photoreduction activities of *n*-decyl-β-D-maltopyranoside-extracted PSI reaction centers from barley (*23*). At saturating FNR concentrations, a turnover number for PSI of 73.5 $e^- s^{-1}$ was obtained. However, these reaction centers contain approximately 0.4 molecule of FNR per P700, and show a turnover of 11 s^{-1} (for PSI) and 29 s^{-1} (for PSI-bound FNR) with $NADP^+$ photoreduction assays, when no additional FNR is included (*23*). These measurements demonstrate that the binding of FNR to PSI reaction centers (probably resulting in a ternary complex, PSI/Fd/FNR) results in the catalysis of relatively high rates of $NADP^+$ photoreduction at low (absolute) FNR concentrations.

Moreover, these authors have shown that the copurified FNR can be cross-linked to PsaE with the zero-length cross-linker *N*-ethyl-3-[3-(dimethylamino)propyl]carbodiimide (EDC) as well as with 3,3′-dithiobis(sulfosuccinimidyl propionate) (DTSSP) (*23*). *n*-Decyl-β-D-maltopyranoside-extracted *Synechocystis* PSI does not contain copurified FNR. The mode of interaction with PSI is therefore probably different in barley, as compared to *Synechocystis*, PCC 6803, the former being more stable in vitro than the latter.

Investigation of Direct Interaction of FNR and PsaE with the Yeast Two-Hybrid System. Since the kinetic model predicts the formation of a transient photosystem I/ferredoxin: $NADP^+$ reductase/ferredoxin ternary complex during linear electron transport, that is dependent on the presence of PsaE, an assay designed to detect protein−protein interaction between FNR and PsaE was carried out. The *Saccharomyces cerevisiae* Gal4-based MATCHMAKER Two-Hybrid system can be used in vivo to detect interactions between proteins, when they are translationally fused to the Gal4 activation domain and the Gal4 DNA-binding domain, respectively (*58*). The fusion proteins are targeted to the nucleus where, if protein−protein interactions induce the formation of a complex that is competent in activation of transcription, a reporter gene is transcribed. The *petH* and the *psaE* genes were amplified by PCR and cloned into the constructs pGAD10 (fusion with activation domain) and pAS2 (fusion with DNA-binding domain), i.e., with either gene as the bait. Co-transformations were performed with all possible combinations of the constructs, testing for background with clone/vector combinations and for dimerization of AD-PetH/DNA-BD-PetH and AD-PsaE/DNA-BD-PsaE fusions. All co-transformants tested were negative with respect to β-galactosidase activity.

DISCUSSION

$NADP^+$ photoreduction rates of PSI reaction centers are the result of a complex set of kinetic parameters. Several transient complexes have to be formed, and a two-electron acceptor has to be reduced by two one-electron carriers. Not all parameters for complex formation and subsequent electron-transfer steps are known. Therefore, after assembling all available kinetic rate constants, a 'simplified' kinetic model was constructed that simulates light-driven electron transport from reduced plastocyanin to $NADP^+$. The overall electron-transfer characteristics were tested and found to simulate the experimentally determined activities reasonably well. Using this model, the behavior of the overall electron-transfer rate was studied as a function of the FNR concentration in the assay. It was found that the affinity of FNR for ferredoxin determines the FNR saturation profile in this assay. Since the experimental observation was an increase in the concentration of FNR that catalyzed 50% of the maximal rate of $NADP^+$ photoreduction in assays with the PsaE-deficient PSI reaction centers, the formation of the ternary complex PSI/Fd/FNR was postulated. This observation was made with the wild-type 47 kDa FNR, that contains the positively charged N-terminal domain. From the observed rates at 100 nM concentration of this wild-type and a truncated form, lacking the N-terminal domain, it is suggested that this domain is not involved in the formation of the ternary complex.

One other possible scenario may explain the altered FNR saturation profile of PsaE-deficient PSI. If an additional 'loss' reaction would take place in the case of mutant reaction centers, higher concentrations of FNR may effectively overcome the flux through such a side-reaction. Possibly PsaE-deficient PSI particles are more active in the reduction of molecular oxygen. However, the maximal rate of $NADP^+$ photoreduction would be affected, rather than the affinity of the system for FNR, if this reaction took place at the reaction center itself. If this reaction would involve reduction of oxygen by ferredoxin, the changed saturation profile might be explained. It is unlikely, however, that removal of the

stromal PsaE subunit would increase the ferredoxin-dependent rate of oxygen reduction.

Using the *Saccharomyces cerevisiae* Two-Hybrid system, it was not possible to demonstrate a direct interaction between PsaE and FNR. The solubility and the level of expression of the fusion proteins were not tested, however. Heterologous expression of PsaE in *E. coli* leads to accumulation of the protein in inclusion bodies (*15*). Therefore, heterologous expression of PsaE or fusion proteins of PsaE in *S. cerevisiae* does not necessarily result in soluble products. In addition, translocation to the nucleus may have been unsuccessful. Interaction between FNR and PsaE remains a probable mechanism to direct the formation of the ternary complex PSI/Fd/FNR. Other techniques should be employed in order to detect this postulated ternary complex.

Given the possibility that a ternary complex of PSI, Fd, and FNR is transiently formed, the question arises what the conformation of the proteins is in the complex. It is known that a chemically cross-linked complex of PSI and ferredoxin is not competent in $NADP^+$ photoreduction in the presence of FNR (*12*). It was found that the same residues of spinach ferredoxin, the acidic cluster Glu92-Glu93-Glu94, cross-link to the PsaD subunit of PSI (*59*), as well as to FNR (*60*), although in the case of the Fd/FNR complex it seems that a highly localized region of ferredoxin is involved in the specific interaction. A mutation of Glu94 (for the *Anabaena* protein; equivalent to Glu93 of the spinach electron carrier) showed dramatic effects on the kinetics, whereas a mutation of Glu95 (equivalent to Glu94 of the spinach Fd) shows almost no effect on electron transfer (*61*). However, it is unlikely that a possible ternary complex is static in its conformation: more likely ferredoxin is mobile within the complex, and the 'high local concentration' of FNR affects a maximal rate of $NADP^+$ reduction at a relatively low concentration of FNR. It should be mentioned that in cyanobacteria a fraction of FNR is bound to the phycobilisomes (*62*) and is therefore already 'concentrated' near the thylakoid.

The existence of a ternary complex has been postulated by others, based on the observation that the rotational correlation time of eosin-labeled FNR, reconstituted into the chloroplast thylakoid membrane, shows a dramatic increase upon the addition of ferredoxin (*63*). However, a possible interpretation of these results would be that the conformation of the ternary complex PSI/ferredoxin/FNR is such that ferredoxin simultaneously binds PSI as well as FNR. In addition, these experiments are complicated by the fact that a ferredoxin binding site exists in the chloroplast thylakoid membrane that is associated with PSI-dependent cyclic electron transport (*64*).

ACKNOWLEDGMENT

We thank Dr. B. Lagoutte for the gift of the *Synechocystis* PCC 6803 *psaE* mutant (FKE2), and Drs. P. Barth and P. Sétif for preliminary communication of the PSI-dependent ferredoxin reduction kinetics of the *psaE* mutant.

NOTE ADDED IN PROOF

Recently an improved X-ray structural model was obtained for *Synechococcus* sp. PSI, including the structure of the PsaE subunit. In contrast to the results obtained with protease accessibility studies, suggesting that the N- and C-termini of the *Synechocystis* PCC 6803 PsaE subunit are buried, both the C- and N-termini turn out to be highly surface-exposed in the improved PSI structure (*65*). This site with excess positive charge could well constitute the binding site for FNR. If this is indeed the binding site, it could also explain the negative results obtained using the two-hybrid method, since PsaE is translationally fused at the N-terminus to the Gal4 DNA binding domain and the Gal4 activation domain in this system.

REFERENCES

1. Schubert, W. D., Klukas, O., Krauss, N., Saenger, W., Fromme, P., and Witt, H. T. (1997) *J. Mol. Biol. 272*, 741−769.
2. Chitnis, P. R. (1996) *Plant Physiol. 111*, 661−669.
3. Bonnerjea, J., and Evans, M. C. W. (1982) *FEBS Lett. 148*, 313−316.
4. Brettel, K., Sétif, P., and Mathis, P. (1986) *FEBS Lett. 203*, 220−224.
5. Biggins, J., and Mathis, P. (1988) *Biochemistry 27*, 1494−1500.
6. Brettel, K. (1997) *Biochim. Biophys. Acta 1318*, 322−373.
7. Krauss, N., Hinrichs, W., Witt, I., Fromme, P., Pritzkow, W., Dauter, Z., Betzel, C., Wilson, K. S., Witt, H. T., and Saenger W. (1993) *Nature 361*, 326−331.
8. Krauss, N., Schubert, W. D., Kuklas, O., Fromme, P., Witt, H., and Saenger, W. (1996) *Nat. Struct. Biol. 3*, 965−973.
9. Kruip, J., Chitnis, P. R., Lagoutte, B., Rögner, M., and Boekema, E. J. (1997*) J. Biol. Chem. 272*, 17061−17069.
10. Sun, J., Xu, Q., Chitnis, V. P., Jin, P., and Chitnis, P. R. (1997) *J. Biol. Chem. 272*, 21793−21802.
11. Xu, Q., Chitnis, V. P., An, K., and Chitnis, P. R. (1995) in *Photosynthesis: From Light to Biosphere* (Mathis, P., Ed.) Vol. II, pp 87−90, Kluwer Academic Publishers, Dordrecht, The Netherlands.
12. Zanetti, G., and Merati, G. (1987) *Eur. J. Biochem. 169*, 143−146.
13. Lelong, C., Boekema, E. J., Kruip, J., Bottin, H., Rögner, M., and Sétif, P. (1996) *EMBO J. 15*, 2160−2168.
14. Mühlenhoff, U., Kruip, J., Bryant, D. A., Rögner, M., Sétif, P., and Boekema, E. (1996) *EMBO J. 15*, 488−497.
15. Falzone, C. J., Kao, Y. H., Zhao, J., Bryant, D. A., and Lecomte, J. T. (1994) *Biochemistry 33*, 6052−6062.
16. Chitnis, P. R., Reilly, P. A., Miedel, M. C., and Nelson, N. (1989) *J. Biol. Chem. 264*, 18374−18380.
17. Rousseau, F., Sétif, P., and Lagoutte, B. (1993) *EMBO J. 12*, 1755−1765.
18. Yu, L., Zhao, J., Muhlenhof, U., Bryant, D. A., and Goldbeck, J. H. (1993) *Plant Physiol. 103*, 171−180.
19. Chitnis, P. R., Chitnis, V. P., Xu, Q., Jung, Y. S., Yu, L., and Goldbeck, J. H. (1995) in *Photosynthesis: From Light to Biosphere* (Mathis, P., Ed.) Vol. II, pp 17−22, Kluwer Academic Publishers, Dordrecht, The Netherlands.
20. Sonoike, K., Hatanaka, H., and Katoh, S. (1993) *Biochim. Biophys. Acta 1141*, 52−57.
21. Xu, Q., Jung, Y. S., Chitnis, V. P., Guikema, J. A., Golbeck, J. H., and Chitnis, P. R. (1994) *J. Biol. Chem. 269*, 21512−21518.
22. Barth, P., Lagoutte, B., and Sétif, P. (1998) *Biochemistry 37*, 16233−16241.
23. Andersen, B., Scheller, H. V., and Moller, B. L. (1992) *FEBS Lett. 311*, 169−173.
24. Rippka, R., Deruelles, J., Waterbury, J. B., Herdman, M., and Stanier, R. Y. (1979) *J. Gen. Microbiol. 111*, 1−61.
25. Marker, A. E. H. (1972) *Freshwater Biol. 2*, 361−385.
26. Forti, G., Melandri, B. A., San Pietro, A., and Ke, B. (1970) *Arch. Biochem. Biophys. 140*, 107−112.
27. Hutber, G. N., Smith, A. J., and Rogers, L. J. (1981) *Phytochemistry 20*, 383−387.

28. Hervás, M., Navarro, F., Navarro, J. A., Chavez, S., Diaz, A., Florencio, F. J., and De la Rosa, M. A. (1993) *FEBS Lett. 319*, 257−260.
29. van Thor, J. J., Hellingwerf, K. J., and Matthijs, H. C. P. (1998) *Plant Mol. Biol. 36*, 353−363.
30. Kaneko, T., Sato, S., Kotani, H., Tanaka, A., Asamizu, E., Nakamura, Y., Miyajima, N., Hirosawa, M., Sugiura, M., Sasamoto, S., Kimura, T., Hosouchi, T., Matsuno, A., Muraki, A., Nakazaki, N., Naruo, K., Okumura, S., Shimpo, S., Takeuchi, C., Wada, T., Watanabe, A., Yamada, M., Yasuda, M., and Tabata, S. (1996) *DNA Res. 3*, 185−209.
31. Briggs, L. M., Pecoraro, V. L., and McIntosh, L. (1990) *Plant Mol. Biol. 15*, 633−642.
32. Lei, S., Lin, H., Wang, S., Callaway, J., and Wilox, G. (1987) *J. Bacteriol. 169*, 4379−4383.
33. Evans, C. G. T., Herbert, D., and Tempest, D. W. (1970) in *Methods in Microbiology* (Norris, J. R., and Ribbons, D. W., Eds.) Vol. 2, pp 277−327, Academic Press, London and New York.
34. Fillat, M. F., Borrias, W. E., and Weisbeek, P. J. (1991) *Biochem. J. 280*, 187−191.
35. Allen, J., and Holmes, N. G. (1986) in *Photosynthesis, Energy Transduction. A Practical Approach* (Hipkins, M. F., and Baker, N. R., Eds.) pp 103−141, IRL Press, Oxford, England.
36. Mendes, P. (1997) *Trends Biochem. Sci. 22*, 361−363.
37. De la Cerda, B., Navarro, J. A., Hervas, M., and De la Rosa, M. A. (1997) *Biochemistry 36*, 10125−10130.
38. Hervás, M., Navarro, J. A., Diaz, A., Bottin, H., and De la Rosa, M. A. (1995) *Biochemistry 34*, 11321−11326.
39. Zhao, J., Snyder, W. B., Muhlenhoff, U., Rhiel, E., Warren, P. V., Golbeck, J. H., and Bryant, D. A. (1993) *Mol. Microbiol. 9*, 183−194.
40. Sétif, P. Q. Y., and Botin, H. (1995) *Biochemistry 34*, 9059−9070.
41. Batie, C. J., and Kamin, H. (1984) *J. Biol. Chem. 259*, 11976−11985.
42. Batie, C. J., and Kamin, H. (1986) *J. Biol. Chem. 261*, 11214−11223.
43. Masaki, R., Yoshikawa, S., and Matsubara. (1982) *Biochim. Biophys. Acta 700*, 101−109.
44. Haehnel, W., Jansen, T., Gause, K., Klosgen, R. B., Stahl, B., Michl, D., Huvermann, B., Karas, M., and Herrmann, R. G. (1994) *EMBO J. 13*, 1028−1038.
45. Romero, A., De la Cerda, B., Varela, P. F., Navarro, J. A., Hervas, M., and De la Rosa, M. A. (1998) *J. Mol. Biol. 275*, 327−336.
46. Vassiliev, I. R., Jung, Y., Yang, F., and Goldbeck, J. H. (1998) *Biophys. J. 74*, 2029−2035.
47. Diaz-Quintana, A., Leibl, W., Bottin, H., and Setif, P. (1998) *Biochemistry 37*, 3429−3439.
48. Bhattacharyya, A. K., Meyer, T. E., and Tollin, G. (1986) *Biochemistry 25*, 4655−4661.
49. Walker, M. C., Pueyo, J. J., Navarro, J. A., Gomez-Moreno, C., and Tollin, G. (1991) *Arch. Biochem. Biophys. 287*, 351−358.
50. Hurley, J. K., Fillat, M., Gomez-Moreno, C., and Tollin, G. (1996) *J. Am. Chem. Soc. 118*, 5526−5531.
51. Martinez-Julvez, M., Hurley, J. K., Tollin, G., Gomez-Moreno, C., and Fillat, M. F. (1996) *Biochim. Biophys. Acta 1297*, 200−206.
52. Batie, C. J., and Kamin, H. (1981) *J. Biol. Chem. 256*, 7756−7763.
53. Medina, M., Martinez-Julvez, M., Hurley, J. K., Tollin, G., and Gomez-Moreno, C. (1998) *Biochemistry 37*, 2715−2728.
54. Hurley, J. K., Weber-Main, A. M., Stankovich, M. T., Benning, M. M., Thoden, J. B., Vanhooke, J. L., Holden, H. M., Chae, Y. K., Xia, B., Cheng, H., Markley, J. L., Martinez-Julvez, M., Gomez-Moreno, C., Schmeits, J. L., and Tollin, G. (1997) *Biochemistry 36*, 11100−11117.
55. Smith, J. M., Smith, W. H., and Knaff, D. B. (1981) *Biochim. Biophys. Acta 635*, 405−411.
56. Maskiewicz, R., and Bielski, B. H. J. (1982) *Biochim. Biophys. Acta 680*, 297−303.
57. Shin, M., Tagawa, K., and Arnon, D. I. (1963) *Biochem. Z. 338*, 84−96.
58. Fields, S., and Song, O. (1989) *Nature 340*, 245−246.
59. Lelong, C., Setif, P., Lagoutte, B., and Bottin, H. (1994) *J. Biol. Chem. 269*, 10034−10039.
60. Vieira, B. J., Colvert, K. K., and Davis, D. J. (1986) *Biochim. Biophys. Acta 851*, 109−122.
61. Hurley, J. K., Salamon, Z., Meyer, T. E., Fitch, J. C., Cusanovich, M. A., Markley, J. L., Cheng, H., Xia, B., Chae, Y. K., Medina, M., Gomez-Moreno, C., and Tolin, G. (1993) *Biochemistry 32*, 9346−9354.
62. Schluchter, W. M., and Bryant, D. A. (1992) *Biochemistry 31*, 3092−3102.
63. Wagner, R., Carrillo, N., Junge, W., and Vallejos, R. H. (1982) *Biochim. Biophys. Acta 680*, 317−330.
64. Bendall, D. S., and Manasse, R. S. (1995) *Biochim. Biophys. Acta 1229*, 23−38.
65. Klukas, O., Schubert, W. D., Jordan, P., Krauss, N., Fromme, P., Witt, H. T., and Saenger, W. (1999) *J. Biol. Chem. 274*, 7351−7360.

BI9903502